analytical chemistry

Article

pubs.acs.org/ac

Persistent Luminescence Strontium Aluminate Nanoparticles as Reporters in Lateral Flow Assays

Andrew S. Paterson,[†] Balakrishnan Raja,[†] Gavin Garvey,[†] Arati Kolhatkar,[§] Anna E. V. Hagström,[†] Katerina Kourentzi,[†] T. Randall Lee,[§] and Richard C. Willson*[,†,‡,∥]

[†]Department of Chemical and Biomolecular Engineering, University of Houston, Houston, Texas 77004, United States

[§]Department of Chemistry, University of Houston, Houston, Texas 77004, United States

[‡]Department of Biology and Biochemistry, University of Houston, Houston, Texas 77004, United States

[∥]Centro de Biotecnología FEMSA, Tecnológico de Monterrey, Campus Monterrey, Monterrey, Nuevo León 64849, Mexico

Supporting Information

ABSTRACT: Demand for highly sensitive, robust diagnostics and environmental monitoring methods has led to extensive research in improving reporter technologies. Inorganic phosphorescent materials exhibiting persistent luminescence are commonly found in electroluminescent displays and glowing paints but are not widely used as reporters in diagnostic assays. Persistent luminescence nanoparticles (PLNPs) offer advantages over conventional photoluminescent probes, including the potential for enhanced sensitivity by collecting time-resolved measurements or images with decreased background autofluorescence while eliminating the need for expensive optical hardware, superior resistance to photobleaching, amenability to quantitation, and facile bioconjugation schemes. We isolated rare-earth doped strontium aluminate PLNPs from larger-particle commercial materials by wet milling and differential sedimentation and water-stabilized the particles by silica encapsulation using a modified Stöber process. Surface treatment with aldehyde silane followed by reductive amination with heterobifunctional amine-poly(ethylene glycol)-carboxyl allowed covalent attachment of proteins to the particles using standard carbodiimide chemistry. NeutrAvidin PLNPs were used in lateral flow assays (LFAs) with biotinylated lysozyme as a model analyte in buffer and monoclonal anti-lysozyme HyHEL-5 antibodies at the test line. Preliminary experiments revealed a limit of detection below 100 pg/mL using the NeutrAvidin PLNPs, which was approximately an order of magnitude more sensitive than colloidal gold.

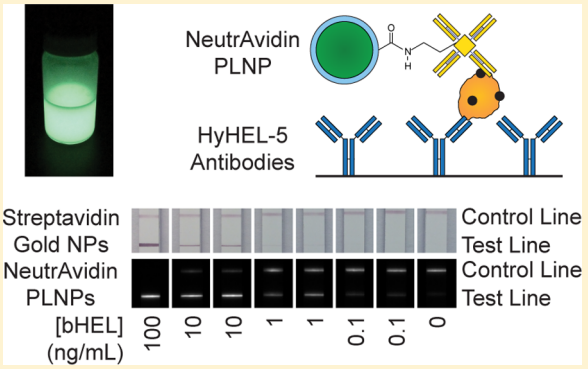

Growing demand for reliable diagnostic tests for pathogens and disease biomarkers in low-resource and point-of-care (POC) settings has led to significant research in developing new assay technologies such as cellphone-based diagnostics[1] and new or improved photoluminescent reporters.[2] One of the more promising assay formats for POC diagnostics is the immunochromatographic lateral flow assay (LFA), which is widely known from its use in home pregnancy tests.[3,4]

LFAs using photoluminescent labels such as fluorescent nanoparticles and quantum dots have been shown to have higher sensitivity and wider dynamic range than LFAs that use conventional gold nanoparticles.[5] The increased sensitivity from photoluminescent reporters, however, is not without drawbacks. Fluorescent dyes are prone to photobleaching, and fluorescence measurements require continuous excitation, which increases the cost and complexity of the readout device.[6] Background autofluorescence at the wavelengths of the reporter's emission can also limit sensitivity.[7,8]

Upconverting phosphors (UCPs) that emit visible light upon excitation by infrared or near-infrared sources have seen increased use in LFAs[9−11] and biological imaging applications[12,13] and offer advantages over conventional fluorescent labels including minimal background autofluorescence and high resistance to photobleaching. However, UCPs have low quantum yields (e.g., 3% for bulk samples of $NaYF_4$:Er^{3+},Yb^{3+} and 0.3% for 100 nm particles),[14] and the efficiency decreases dramatically at low optical power densities of the excitation source.[15] Therefore, many readers for UCP assays are complex, using laser diodes for excitation, in combination with other hardware such as lenses, filters, photomultiplier tubes, preamplifiers, and stepper motors.[16−20]

One strategy to simultaneously reduce the cost of the reader by eliminating the need for optical filters and decrease background autofluorescence is to carry out time-resolved measurements wherein a reporter with a longer emission lifetime than typical fluorophores (e.g., 100 μs compared to 10

Received: April 7, 2014
Accepted: September 10, 2014
Published: September 23, 2014

   dx.doi.org/10.1021/ac5012624 | *Anal. Chem.* 2014, 86, 9481−9488

ns)[6,21] is used, and a time delay between excitation and measurement is introduced to allow for decay of the background signal.[7,8,22,23] Phosphorescent metal chelates typically used in time-resolved assays, however, have photostability issues[24] and must be observed during their short remaining period of brightness after a carefully defined delay time.

Here, we introduce assay reporters based on persistent luminescence nanoparticles (PLNPs) that emit intense visible light for several minutes after excitation. Persistent luminescence (sometimes also referred to as phosphorescence or long-lasting phosphorescence) in solids generally arises when an inorganic host material is doped with small amounts of an activator metal, which alters the electronic structure, resulting in trapping of charge carriers in metastable states upon excitation.[7,25−27] Gradual detrapping by thermal activation causes luminescence from electron−hole recombination.[26−30] A wide variety of materials exhibiting persistent luminescence have been synthesized, including the relatively common zinc sulfide phosphors. Strontium aluminate doped with europium and dysprosium ($SrAl_2O_4$:Eu^{2+},Dy^{3+}) is a persistent luminescence material with a long and bright afterglow that is observable by eye for several hours after excitation[31] and is highly resistant to photobleaching with only a 20% loss in luminescence intensity after constant exposure to 370 nm UV light for 2 weeks,[32] making it popular in applications like luminescent paint. It is one of the brightest known persistent luminescence materials, with an afterglow intensity about ten times that of ZnS:Cu,Co phosphors.[31] Strontium aluminate has been extensively studied to understand the mechanisms that give rise to its persistent luminescence,[30,33] to assess the effects of concentration and type of rare earth dopants on the emission wavelength, intensity, and lifetime, to examine changes in the luminescence properties by substitution of strontium for other alkaline earth metals,[34] and to improve synthesis strategies.[35−37]

PLNPs have recently appeared as reporters for *in vitro* binding assays[38] and *in vivo* imaging[39−41] but have not yet been used in LFAs to the best of our knowledge. Here, we demonstrate the use of strontium aluminate PLNPs as reporters in LFAs with biotinylated hen egg lysozyme (bHEL) as a model analyte. Size reduction of the phosphors by wet milling and separation by centrifugal settling, followed by silica encapsulation for water-stability, yielded particles small enough to move in the LFA membranes while retaining luminescence bright enough for low-picomolar (7 pM) bHEL detection without the need for optical filters or continuous excitation. Our results show that PLNPs are a promising class of materials for LFAs and potentially other *in vitro* diagnostics applications requiring robustness and high sensitivity. Developing assays with PLNPs as reporters could lead to more sensitive point-of-care tests with significantly cheaper and simpler field-portable readers.

EXPERIMENTAL SECTION

Materials and Reagents. Tetraethyl orthosilicate (TEOS), 96% 1,2-bis(triethoxysilyl)ethane (BTEOSE), hydroxylamine hydrochloride, 3350 g/mol polyethylene glycol (PEG), 2-(*N*-Morpholino)ethanesulfonic acid sodium salt (MES), 99.9% dimethyl sulfoxide (DMSO), *N*-hydroxysuccinimide (NHS), Tween 20, Triton X-100, bovine serum albumin (BSA), and lysozyme from chicken egg white were purchased from Sigma-Aldrich. Sodium cyanoborohydride and 1-ethyl-3-(3-dimethylaminopropyl)carbodiimide (EDC) were purchased from Thermo Scientific. Ethyl acetate, ammonium acetate, and 28−30% ammonium hydroxide were obtained from EM Science (Gibbstown, N.J.). Other reagents and their respective suppliers were glacial acetic acid (Macron), triethoxysilylbutyraldehyde (TESBA; Gelest), 3400 g/mol amine-polyethylene glycol-carboxyl (NH_2-PEG-COOH; NANOCS), anhydrous ethanol (VWR), dibasic potassium phosphate (Spectrum), monobasic potassium phosphate (J. T. Baker), and phosphate buffered saline tablets (Bioline). Sodium hydroxide (Macron) and hydrochloric acid (Fisher Scientific) were used for titrating buffers to the desired pH. Buffers were prepared with deionized water (Millipore Milli-Q) and filtered with nonpyrogenic sterile polystyrene filters (Corning Product #430625). The phosphorescent strontium aluminate powder used in all LFAs was purchased from Glow Inc. (Ultra Green v10 Glow in the Dark Powder). Phosphors obtained from Ambient Glow Technology (Product #AGT-SYS-F) were used in preliminary milling and silica encapsulation experiments. BD Falcon Microtest 96-well black plates were used for luminescence characterization measurements (BD Biosciences, Franklin Lakes, NJ). NeutrAvidin was purchased from Thermo Scientific (Product #31000). Streptavidin gold nanoparticles, 40 nm, were purchased from DCN Diagnostics (Carlsbad, CA; Product #PACG-060). Mouse anti-lysozyme monoclonal HyHEL-5 antibodies were produced from hybridoma cells and purified by Protein G Affinity Chromatography by Biovest/National Cell Culture Center (Minneapolis, MN).

Biotinylation of Lysozyme. BSA and lysozyme were biotinylated at room temperature for 90 min using EZ-Link Sulfo-NHS-LC-Biotin (Thermo Scientific, Product #21335). Excess biotinylation reagent was removed using Zeba Spin Desalting Columns (Thermo Scientific, Product #89892). The number of biotin molecules per protein was estimated by a HABA assay using NeutrAvidin, premade HABA solution from Thermo Scientific (Product #1854180), and absorbance measurements taken with a NanoDrop ND-1000 Spectrophotometer. HABA assay results indicated an average biotinylation of 1.2 biotin/protein for BSA and 2.5 biotin/protein for lysozyme.

Milling and Fractionation. Typically 3−5 g of phosphorescent strontium aluminate powder was dispersed in 30−50 mL of ethyl acetate in a ceramic milling jar (U.S. Stoneware Roalox Alumina-Fortified Grinding Jar, Size 000, 0.3 Liters) with 15 large (3/8 in. diameter × 3/8 in. length) and 10 small (1/4 in. diameter × 1/4 in. length) magnesia stabilized zirconia cylinders as grinding media and placed on a mill (U.S. Stoneware, Model 755RMV Unitized Jar Mill) at 60% power (≈110 rpm) for 7−9 days. After wet milling, the colloidal dispersion of phosphors was collected and the ethyl acetate was removed by room temperature evaporation. Dry milled phosphorescent powder was then dispersed in ethanol, and fractions with different size distributions were isolated by differential centrifugal sedimentation with a Beckman Coulter Avanti J-E centrifuge in 50 mL centrifuge tubes. The centrifugal settling process was repeated until the concentration of particles in a fraction approached 2−4 mg/mL, as measured by evaporating the ethanol from a known volume of a particle suspension and weighing the remaining dry mass with a Mettler Toledo XS64 analytical balance.

Silica Encapsulation. Typically, 1.6 mg of dry milled size-fractionated phosphorescent particles was suspended in 1 mL of anhydrous ethanol in a 2 mL microcentrifuge tube. A solution containing approximately 222 μL of ethanol, 247 μL of

dx.doi.org/10.1021/ac5012624 | Anal. Chem. 2014, 86, 9481−9488

DI water, and 6.7 μL of TEOS was prepared, vigorously agitated, and then added immediately to the suspension of phosphors in ethanol. The tube with the particles was then placed in a bath sonicator (Fisher Scientific FS30) for 5 min, and afterward, 25 μL of aqueous ammonium hydroxide (28−30%) was added to the reaction mixture, bringing the final volume to 1.5 mL. The calculated concentrations of TEOS and ammonia were 20 mM and 0.25 M, respectively, with approximately 17.5% v/v water and 81.4% v/v ethanol. After adding the ammonium hydroxide, the particles were sonicated for an additional 30 min and then placed on a room temperature rotator for 7.5 h to keep the particles suspended, with an overall silica encapsulation time of approximately 8 h. Silica encapsulation was stopped by centrifuging to induce settling (Eppendorf Centrifuge 5418), removing the supernatant, and resuspending the particles in ethanol by vigorous agitation with a Fisher Vortex Genie 2 and sonication. After 4 wash cycles, the particles were dried in a Savant SpeedVac Concentrator SVC100H at 36 °C under reduced pressure for 1 h.

Aldehyde Functionalization. Aldehydes were introduced on the surfaces of the silica encapsulated particles by reacting the particles with TESBA in the presence of BTEOSE as a crosslinker for enhanced water stability of the surface aldehydes. Aldehyde functionalization was carried out with 50 mM TESBA and 25 mM BTEOSE in 5% v/v DI water in ethanol, with 1.6 mg (dry strontium aluminate basis) of encapsulated particles suspended in a 1 mL reaction volume. The particles were sonicated during the first 20 min of the reaction and placed on a rotator at room temperature for an additional 40 min. The particles were then washed in ethanol. After 3 wash cycles, the particles were dried for 20 min in a Savant SpeedVac Concentrator SVC100H at 36 °C under reduced pressure.

PEG-Carboxylation. A stock solution of 20 mM heterobifunctional 3400 g/mol NH_2-PEG-COOH was prepared in DMSO. Conjugation of the PEG chains to the particle surfaces was carried out by reductive amination in which aldehyde functionalized particles were dispersed in 500 μL of phosphate buffer (115 mM K_2HPO_4, 15 mM KH_2PO_4, adjusted to pH 7.8), in the presence of 250 mM sodium cyanoborohydride with 0.5 mM NH_2-PEG-COOH diluted from the stock solution. The particles were placed on a Cole-Parmer Roto-Torque rotator for 24 h at room temperature and then washed at least three times in deionized water.

Bioconjugation. Bioconjugation was carried out using carbodiimide chemistry. Carboxylated phosphors were washed in 50 mM, pH 5.8 MES buffer and then suspended in MES buffer with 60 mM EDC and 30 mM NHS for 30 min to activate the carboxyl groups. After activation, the particles were centrifuged, the supernatant was removed, and the particles were resuspended in 500 μL of pH 7.4 PBS with 0.1 mg/mL NeutrAvidin and placed on a rotator for 5 h. After bioconjugation, any remaining activated carboxyls were quenched by suspending the particles in 0.1 M hydroxylamine in PBS for an additional 2 h.

Particle Size Analysis. Optical microscopy images of the particles were taken with a Nikon Eclipse LV100D-U at various times during the wet milling process to assess the extent of size reduction. During fractionation experiments, the average particle size was monitored using dynamic light scattering (DLS) with a Brookhaven BI-200SM. Final size distributions of unencapsulated phosphors were obtained using an Affinity Biosensors Archimedes Particle Metrology system, with the particles suspended in anhydrous ethanol. Scanning electron microscopy (SEM) images were taken with a LEO 1525 field emission SEM for size and morphology analysis.

X-ray Photoelectron Spectroscopy (XPS), Energy Dispersive X-ray Spectroscopy (EDS), and Transmission Electron Microscopy (TEM). Qualitative elemental analysis of the as-purchased phosphorescent powder was carried out with a JEOL JSM-6330F field emission SEM equipped with an AMETEK EDAX Octane Pro energy dispersive X-ray spectroscopy (EDS) system to confirm the identity of the rare earth dopants and verify that the host material is strontium aluminate. EDS data are provided in the Supporting Information (Figure S11). XPS was used for elemental analysis and surface characterization of particles. Spectra were collected with a Physical Electronics PHI 5700 system equipped with a monochromatic Al Kα X-ray source (1486.7 eV) at a 45° takeoff angle. Particles were spotted on a gold film on a silicon wafer. Silica-coated phosphors were characterized by TEM (JEOL, Model JEOL-2000 FX, operating at 200 kV). For the TEM analyses, silica-coated phosphors suspended in ethanol were deposited on a 300-mesh holey carbon-coated copper grid and allowed to dry at room temperature before imaging.

Luminescence Decay Kinetics. Luminescence decay kinetics were measured with a Tecan Infinite M200 Pro microplate reader in luminescence mode with no emission filters. Phosphors were excited under a Chauvet 18 in., 370 nm, 15 W UV light for 3 min and were immediately loaded into the instrument to commence measurement. Each decay curve was normalized by its initial intensity.

LFA Membrane Preparation. Whatman (GE Healthcare) FF80HP nitrocellulose membranes were used in all LFAs. A ClaremontBio Lateral Flow Reagent Dispenser powered by a programmable BK Precision 9130 DC power supply was used in combination with a Chemyx Inc. Fusion 200 syringe pump to spot proteins on the nitrocellulose membranes. HyHEL-5 antibodies were diluted to a concentration of 0.8 mg/mL in pH 6.9 phosphate buffer (15 mM KH_2PO_4, 15 mM K_2HPO_4) and loaded into 1 mL BD Luer-Lok syringes, then connected to the syringe pump, and dispensed at a rate of 0.2 mL/min with a 4 cm/s head speed. Biotinylated BSA was diluted to 0.25 mg/mL in pH 5.4 ammonium acetate buffer and dispensed at the same flow rate and speed as the antibodies. Membranes were dried for 30 min at 37 °C in a Robbins Scientific Micro Hybridization Incubator 2000. The membranes were assembled on 0.010 in. adhesive cards from DCN Diagnostics (Part #MIBA-020) with Whatman Standard 14 sample pads and Whatman CF5 absorbent pads. The LFA strips were cut with a desktop paper cutter such that the nitrocellulose part of the assembly was approximately 0.5 × 4 cm.

LFA Image Acquisition and Analysis. Typically 8−10 LFA strips were stuck on a 120 × 120 mm square Petri dish from Greiner (Catalog #688102) using double-sided adhesive tape. A buffer containing (wt %) 0.5% nonfat dry milk, 2% Tween-20, and 0.3% PEG-3350 in PBS was prepared for analyte dilutions. A wash buffer containing 0.3% PEG-3350, 1% Triton X-100, and 1.5% Tween 20 in PBS was also prepared. NeutrAvidin PLNPs were diluted to a concentration of 0.2 mg/mL (strontium aluminate dry mass basis) in wash buffer. Each LFA was run by applying 50 μL of analyte to the sample pad, followed by 25 μL of wash buffer, 25 μL of 0.2 mg/mL NeutrAvidin PLNPs, and 100 μL of wash buffer sequentially. The strips from a given dilution series were imaged

dx.doi.org/10.1021/ac5012624 | Anal. Chem. 2014, 86, 9481−9488

simultaneously with an Alpha Innotech FluorChem SP gel documentation system. LFA strips were first excited for 3 min with a 370 nm Chauvet 18 in., 15 W UV light and were then loaded into the FluorChem and imaged with an 8 min exposure time in high sensitivity/normal resolution mode. It should be noted that a shorter exposure time (<1 min) can be used for imaging, albeit with a lower signal-to-noise ratio. The approximate time delay between excitation and the commencing image acquisition was 10 s. The Chauvet light source was used in the LFA experiments herein to ensure even excitation across all strips. However, smaller 2.5 mW low cost LEDs (Thorlabs, Item #LED370E) have been used to effectively excite phosphors in single LFA strips in other experiments with shorter excitation times (<30 s). Boxes of equivalent size were drawn around the test line and control line of each strip in ImageJ to calculate the average pixel intensities that were used in Figure 6C and the statistical analysis. The LFA procedure was the same for assays run with Streptavidin gold nanoparticles, except 25 μL of Streptavidin gold at a concentration of $\approx 8.6 \times 10^{10}$ particles/mL was applied to each strip instead of NeutrAvidin PLNPs. Images of the LFA strips run with gold nanoparticles were acquired with an iPhone 5s, and line scans of the strips were obtained using ImageJ and an Epson Perfection V600 scanner.

RESULTS AND DISCUSSION

Particle Size Reduction and Analysis. The commercial phosphorescent strontium aluminate powder consists of large particles with effective diameters much greater than 10 μm, which settle rapidly upon dispersion in liquid. For most diagnostics applications, the particles must be suspendable in liquid without significant sedimentation over short times, and for LFAs, the particles must pass through membranes with pore sizes ranging from less than one micrometer to a few micrometers. The mean particle size was reduced by wet milling in ethyl acetate with zirconia grinding media. SEM (Figure 1A) and optical microscopy (Figure S1, Supporting Information) images show extensive size reduction after 24 h of wet milling, with few particles greater than 10 μm remaining. Milling was extended to further reduce the average particle size and polydispersity. The milled phosphors retain visible luminescence, as shown in the image of milled phosphors dispersed in ethanol (Figure 1B).

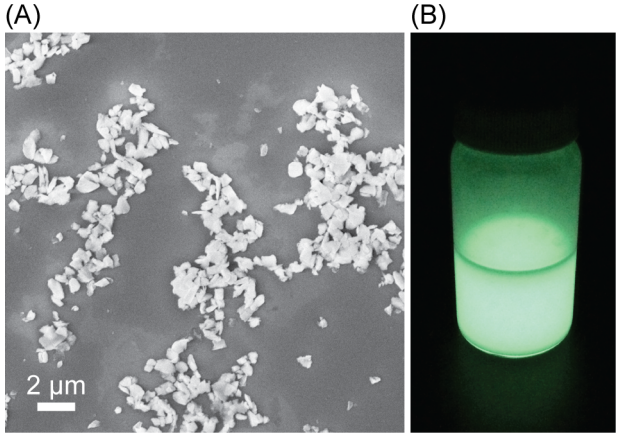

Figure 1. (A) SEM image of phosphors after 9 days of wet milling in ethyl acetate with zirconia grinding media. (B) Image showing luminescence from milled phosphors dispersed in ethanol after 30 s of excitation with 370 nm UV light.

Differential sedimentation was used to isolate fractions of phosphors with lower polydispersity and smaller mean diameters to improve performance of the particles in LFAs and for greater consistency in chemical functionalization. A suspended microchannel resonator (Archimedes, Affinity Biosensors LLC) was used for size characterization of the fractionated phosphors at single-particle resolution with low-femtogram sensitivity.[42,43] The instrument incorporates microfluidics to control the flow of individual nanoparticles through a channel in a resonating cantilever vibrating in vacuum, and an optoelectronic detection system measures resonant frequency shifts which are used to calculate the nanoparticle buoyant mass relative to the volume of the displaced liquid. Equivalent spherical diameters for the particles were calculated from the data giving an approximately normal distribution with a mean and standard deviation of 248 and 81 nm, respectively. The size distribution in Figure 2 was used to estimate the total particle number in a measured dry mass.

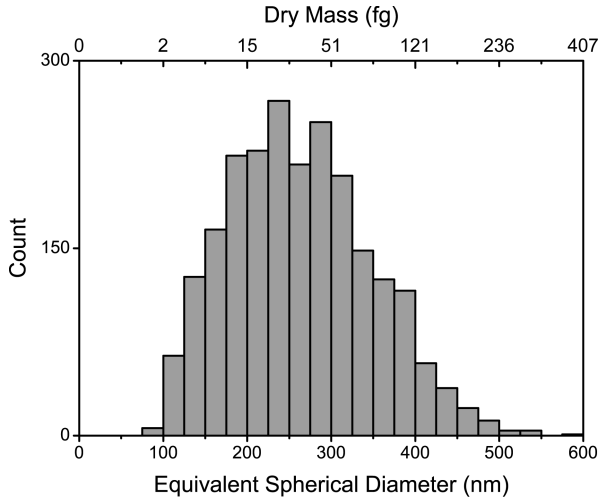

Figure 2. Single-particle size distribution of fractionated milled phosphors measured with Archimedes microchannel resonator; median = 244 nm, mean = 248 nm, and standard deviation = 81 nm.

Luminescence Decay Properties. Mechanical milling is known to induce structural and atomic scale defects in solids, and the luminescence properties of inorganic phosphors are strongly affected by crystallinity. Defects can increase the relative rates of nonradiative relaxation processes, reducing the luminescence lifetime and quantum efficiency.[44,45] We measured the luminescence decay curves of milled and as-purchased unmilled strontium aluminate phosphors to examine the effects of milling. The luminescence intensity decreases to 10% of its initial measured value in approximately 13.4 and 7.0 min for unmilled and milled phosphors, respectively, after excitation with a 370 nm UV light (Figure 3). The shorter lifetime of the milled phosphors may arise from increased surface dead layer effects, as nonradiative recombination processes may be more common at the surface.[44] Although milling slightly decreased the emission lifetime, the milled particles retain a lifetime long enough for detection without continuous excitation and are bright enough that approximately 10 ng of the particles can be detected in a microplate reader in luminescence mode (Figure S2, Supporting Information).

dx.doi.org/10.1021/ac5012624 | Anal. Chem. 2014, 86, 9481−9488

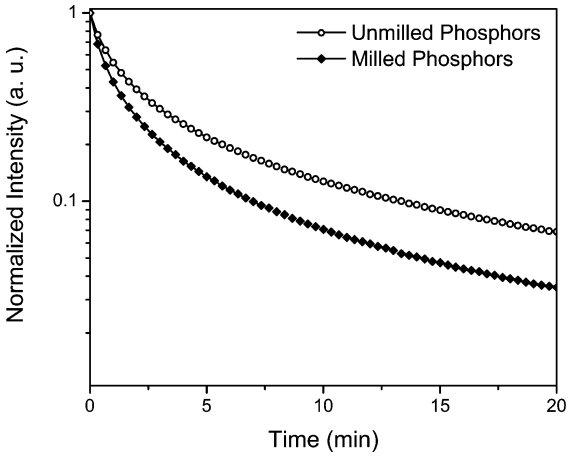

Figure 3. Luminescence decay curves normalized to the same initial intensity for milled and unmilled phosphors after a 3 min excitation under a 370 nm UV light.

Silica Encapsulation. Strontium aluminate readily hydrolyzes in water to form nonluminescent aluminum hydroxide precipitate and soluble strontium hydroxide.[46] Several approaches have been investigated for improving water stability of strontium aluminate including encapsulation with silica by sol–gel or precipitation techniques,[46] direct reaction with phosphoric acid,[47] and encapsulation with triethanolamine.[48] Due to the wide use of trialkoxysilanes in bioconjugate chemistry and their high compatibility with silica surfaces, we used a modified Stöber process to form a silica shell around the phosphors.

Typical Stöber protocols for encapsulating particles in silica involve the reaction of TEOS in a ≈20% v/v water in ethanol solution with ammonium hydroxide added as a catalyst. Since water is an essential reactant in the Stöber process, but also degrades strontium aluminate, we varied the initial water concentration to determine the optimum concentration. When the total initial water concentration was decreased to 3.4% v/v in ethanol with 20 mM TEOS and 0.5 M NH_3, the particles were not stable for more than a day in deionized (DI) water; increasing the TEOS concentration to 40 mM did not improve stability. Phosphors that were encapsulated using conditions similar to typical Stöber recipes in literature[49] with a high water/TEOS molar ratio at approximately ≈18% v/v water in ethanol were the most resistant to hydrolytic degradation. Hydrolysis of alkoxy groups is known to be reversible,[50−53] so it is likely that a water concentration much greater than the stoichiometric ratio is needed to drive TEOS hydrolysis to completion and form an effective silica barrier around the phosphorescent core. Details on silica encapsulation are provided in the Supporting Information. All phosphors referred to hereafter were encapsulated with silica using the protocol described in the Experimental Section. Phosphors treated with this protocol showed no significant loss of luminescence or increase in pH over 2 weeks after resuspending the particles in DI water, indicating negligible hydrolysis.

Surface Functionalization and Characterization. Trialkoxysilanes are commonly used for modifying the surface chemistry of glass and silica for covalent attachment of biological macromolecules.[54] Silica encapsulated phosphors were reacted with TESBA to introduce aldehydes on the surface for reactions with primary amines. Initially, proteins were directly coupled to the surface aldehydes, but we found that introducing a bifunctional (PEG) spacer with a carboxylic acid and an amine at opposite terminal ends of the chain, followed by protein coupling with carbodiimide chemistry, resulted in particles that were more easily suspended in aqueous buffer and had improved transport through nitrocellulose membranes. BTEOSE was added during aldehyde functionalization, as bridged silane coupling agents have been shown to reduce the loss of PEG chains grafted onto silica nanoparticles by trialkoxysilanes.[55] A schematic showing the surface chemistry of the phosphors is provided in the Supporting Information (Figure S6).

X-ray photoelectron spectroscopy (XPS) data from different stages of the functionalization process are presented in Figure 4. Spectra of unencapsulated milled phosphors are similar to

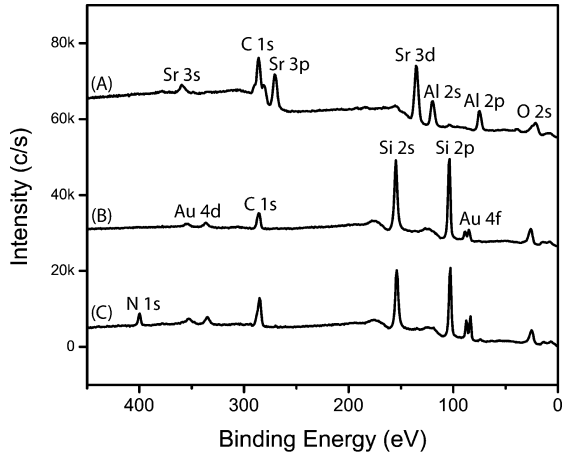

Figure 4. XPS survey spectra of strontium aluminate phosphors at different stages of functionalization spotted on a gold substrate. (A) Milled phosphors prior to silica encapsulation. (B) Strontium aluminate phosphors after silica encapsulation. (C) Silica encapsulated phosphors after functionalization with PEG and NeutrAvidin.

those previously reported for strontium aluminate,[35] with Sr 3s, $3p_{3/2}$, and 3d peaks at 359.6, 270.8, and 135.6 eV and Al 2s and 2p peaks at 119.6 and 74.8 eV, respectively. The peak at 286 eV is predominately C 1s with contributions from the adjacent Sr $3p_{1/2}$ peak at 280.8 eV.[56] The C 1s peak could be from impurities incorporated into the host material during synthesis and surface contamination introduced during milling and fractionation. Phosphors encapsulated by the modified Stöber process showed prominent Si 2s and 2p peaks at 154.8 and 103.6 eV, respectively, and significantly reduced Sr and Al peaks, indicating that the particles are encapsulated in silica with little of the phosphorescent core material exposed at the surface. Analysis of TEM images of the nanoparticles revealed an approximate silica shell thickness of 50 nm (Figure S5, Supporting Information). Phosphors functionalized with TESBA and BTEOSE, followed by PEG and NeutrAvidin, show a N 1s peak at 399.6 eV demonstrating conjugation of proteins to the surface. The high resolution C 1s peak of the NeutrAvidin phosphors shows a small shoulder at 287.3 eV shifted to a higher binding energy by approximately 3 eV from the main peak at 284.3 eV, indicating the presence of carbonyls from amides and carboxylic acids of the attached proteins (Figure 5).[57,58]

Lateral Flow Assay. We used biotinylated hen egg lysozyme (bHEL) as a model analyte to demonstrate the use of strontium aluminate PLNPs as LFA reporters. Nitrocellulose

dx.doi.org/10.1021/ac5012624 | Anal. Chem. 2014, 86, 9481−9488

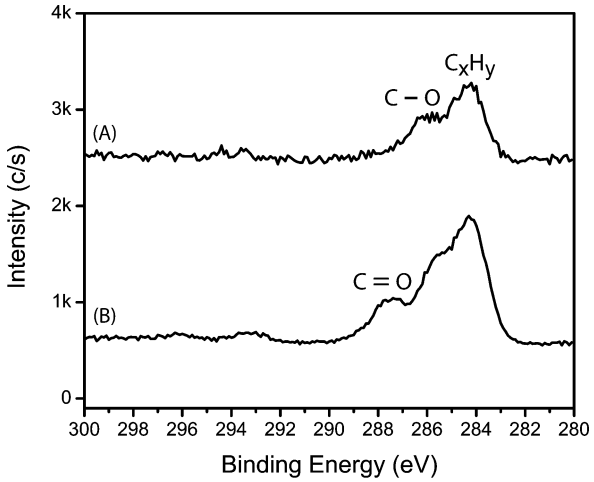

Figure 5. High-resolution XPS spectra of C 1s peaks. (A) Silica encapsulated phosphors. (B) Silica encapsulated phosphors after functionalization with PEG and NeutrAvidin.

strips were functionalized with a test line containing immobilized HyHEL-5 monoclonal anti-lysozyme antibodies.[59] PLNPs functionalized with NeutrAvidin were used as reporters. Bovine serum albumin (BSA) was biotinylated and adsorbed on the nitrocellulose to serve as a control line to capture NeutrAvidin PLNPs that flowed past the test line. A schematic depicting the binding of a NeutrAvidin phosphor to bHEL captured by antibodies at the test line is shown in Figure 6A. Serial dilutions of bHEL were prepared in PBS containing 0.5% nonfat dry milk, 2% Tween-20, and 0.3% PEG-3350. For LFAs run with PLNPs, the strips from a given dilution series were excited under a 370 nm UV light for 3 min and then transferred to a standard gel reader for imaging. Figure 6B shows a comparison between LFAs run with NeutrAvidin PLNPs and Streptavidin gold nanoparticles as the reporter. The visible detection limit for Streptavidin gold nanoparticles is close to 1 ng/mL of bHEL, although the test line signal at this concentration is weak and barely discernible by eye. Line scans of the Streptavidin gold LFA strips are shown in Figure S9, Supporting Information. For LFAs run with NeutrAvidin PLNPs, ratios of the test line intensity to the control line intensity were calculated for each strip, and the average intensity ratio and standard deviation from 4 independent trials are shown in Figure 6C.[9,10] Examination of the images in Figure 6B,C reveals that bHEL concentrations at or above 1 ng/mL are readily detectable. The no-target controls show modest nonspecific binding of the phosphors at the test line. A one-tailed *t* test[60] reveals that the difference in the mean intensity ratio between the 0.1 ng/mL samples and the no-target controls is statistically significant at $\alpha = 0.025$, with a *p*-value of 0.0057. The mean intensity ratio of the 0.1 ng/mL samples is greater than 3 times the standard deviation plus the mean of the no-target controls. The limit of detection for LFAs run with PLNPs is therefore slightly below 0.1 ng/mL (7 pM), approximately an order of magnitude more sensitive than the Streptavidin gold nanoparticles.

Despite the low limit of detection, there is still a small but observable amount of luminescence from PLNPs bound at the test line in the no-target controls. It is conceivable that the background could be reduced and a lower limit of detection achieved using alternate surface modification strategies that result in lower nonspecific binding[61] or further optimization of the PEG grafting protocols.[62] The gel imager and UV illumination system used for readout of the PLNP LFAs is not optimized for time-resolved photoluminescence and is not ideal for point-of-care testing. However, various point-of-care reader designs could be implemented to have a shorter, better-controlled time delay between excitation and imaging, which could improve the limit of detection by increasing the luminescence signal while decreasing its variability between assays. Light detection with a photomultiplier tube or avalanche photodiode instead of a digital camera for readout could also increase the analytical sensitivity. The nanoparticles used in the present work are relatively large and polydisperse compared to typical LFA reporters. Future work may lead to smaller, more monodisperse PLNPs that also possess the luminescence properties necessary for sensitive *in vitro* diagnostics.

■ CONCLUSIONS

We have demonstrated LFAs based on persistent luminescence strontium aluminate nanoparticles. The particles are highly photostable, and the silica shell preserves the luminescence

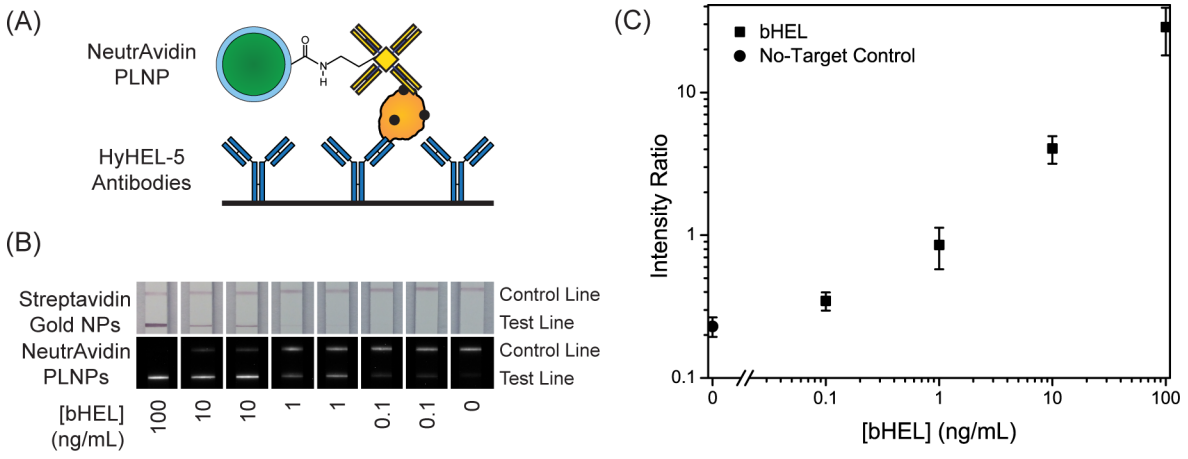

Figure 6. (A) Schematic of test line showing NeutrAvidin phosphor bound to bHEL captured by anti-HEL antibodies. (B) LFA strips showing bHEL serial dilutions with duplicates and detection with Streptavidin gold nanoparticles (top) and NeutrAvidin PLNPs (bottom). (C) Average intensity ratios ($I_{\text{test line}}/I_{\text{control line}}$) and ± standard deviations at different bHEL concentrations from LFA experiments with NeutrAvidin PLNPs (n = 4).

dx.doi.org/10.1021/ac5012624 | *Anal. Chem.* 2014, 86, 9481−9488

properties by preventing hydrolytic degradation. Surface functionalization of the particles can be achieved using standard methods and could readily be extended to bioconjugation of antibodies, nucleic acids, or other biomolecules for the detection of various analytes. We demonstrated that the particles can be used in LFAs for rapid detection with high sensitivity without continuous excitation. The long luminescence lifetime can potentially alleviate design constraints on point-of-care diagnostic devices by eliminating the need for optical filters required for fluorescence measurements and also offers the advantage of reduced background autofluorescence when the particles are used in a time-resolved manner. Future work with phosphorescent strontium aluminate and other persistent luminescence materials could lead to a new class of reporters for diagnostics and environmental monitoring.

■ ASSOCIATED CONTENT

Supporting Information

Details on milling, silica encapsulation, and surface chemistry; test line intensity profiles and additional LFA images, EDS spectrum of purchased strontium aluminate, excitation and emission spectra, and serial dilution of particles detected with a microplate reader. This material is available free of charge via the Internet at http://pubs.acs.org.

■ AUTHOR INFORMATION

Corresponding Author

*Phone:+1 713-743-4308. Fax: +1 713-743-4323. E-mail: willson@uh.edu.

Notes

The authors declare the following competing financial interest(s): A.S. Paterson and R.C. Willson are inventors on patent applications potentially covering the use of nanophosphors in lateral flow assays. A.S. Paterson, B. Raja, and G. Garvey are co-founders of a company that intends to commercialize the technology discussed in this manuscript.

■ ACKNOWLEDGMENTS

The authors thank K. Carpenter, R.-P. Sawh, and R. Weinstein of the University of Houston Institute for Beam Particle Dynamics for allowing access to the ball mill and assisting in the milling process. The authors thank the staff at the Texas Center for Superconductivity at the University of Houston for assistance with TEM and EDS. The authors also thank G. Stein (University of Houston, Department of Chemical & Biomolecular Engineering) for allowing access to the optical microscope. This research was funded in parts by the NIAID/NIH (Grant No. U54 AI057156), the Welch Foundation (Grant No. E-1264), and the Huffington-Woestemeyer professorship. Its contents are solely the responsibility of the authors and do not necessarily represent the official views of the RCE Programs Office, NIAID, or NIH. Postdoctoral scholarships to A.E.V. Hagström from the Olle Engkvist Byggmästare foundation and the Carl Trygger foundation are gratefully acknowledged. T.R. Lee thanks the Robert A. Welch Foundation (E-1320) and the Texas Center for Superconductivity at the University of Houston for generous financial support.

■ REFERENCES

(1) Mudanyali, O.; Dimitrov, S.; Sikora, U.; Padmanabhan, S.; Navruz, I.; Ozcan, A. *Lab Chip* **2012**, *12*, 2678−2686.
(2) Bouzigues, C.; Gacoin, T.; Alexandrou, A. *ACS Nano* **2011**, *5*, 8488−8505.
(3) Posthuma-Trumpie, G. A.; Korf, J.; van Amerongen, A. *Anal. Bioanal. Chem.* **2009**, *393*, 569−582.
(4) Rosen, S. In *Lateral Flow Immunoassay*; Wong, R. C., Tse, H. Y., Eds.; Springer: New York, 2009.
(5) Lee, L.; Nordman, E.; Johnson, M.; Oldham, M. *Biosensors* **2013**, *3*, 360−373.
(6) Song, X.; Knotts, M. *Anal. Chim. Acta* **2008**, *626*, 186−192.
(7) Maldiney, T.; Scherman, D.; Richard, C. In *Functional Nanoparticles for Bioanalysis, Nanomedicine, and Bioelectronic Devices*; Hepel, M., Zhong, C.-J., Eds.; American Chemical Society: Washington, DC, 2012; Vol. *2*, pp 1−25.
(8) Juntunen, E.; Myyryläinen, T.; Salminen, T.; Soukka, T.; Pettersson, K. *Anal. Biochem.* **2012**, *428*, 31−38.
(9) Hampl, J.; Hall, M.; Mufti, N. A.; Yao, Y.-m. M.; MacQueen, D. B.; Wright, W. H.; Cooper, D. E. *Anal. Biochem.* **2001**, *288*, 176−187.
(10) Corstjens, P.; Zuiderwijk, M.; Brink, A.; Li, S.; Feindt, H.; Niedbala, R. S.; Tanke, H. *Clin. Chem.* **2001**, *47*, 1885−1893.
(11) Corstjens, P. L. A. M.; Zuiderwijk, M.; Nilsson, M.; Feindt, H.; Niedbala, R. S.; Tanke, H. J. *Anal. Biochem.* **2003**, *312*, 191−200.
(12) Chatterjee, D. K.; Gnanasammandhan, M. K.; Zhang, Y. *Small* **2010**, *6*, 2781−2795.
(13) Chatterjee, D. K.; Rufaihah, A. J.; Zhang, Y. *Biomaterials* **2008**, *29*, 937−943.
(14) Boyer, J.-C.; van Veggel, F. C. J. M. *Nanoscale* **2010**, *2*, 1417−1419.
(15) Liu, H.; Xu, C. T.; Lindgren, D.; Xie, H.; Thomas, D.; Gundlach, C.; Andersson-Engelsa, S. *Nanoscale* **2013**, *5*, 4770−4775.
(16) Cooper, D. E.; D'Andrea, A.; Faris, G. W.; MacQueen, B.; Wright, W. H. In *Immunoassay and other Bioanalytical Techniques*; van Emon, J. M., Ed.; CRC Press: Boca Raton, 2007; pp 217−246.
(17) Niedbala, R. S.; Feindt, H.; Kardos, K.; Vail, T.; Burton, J.; Bielska, B.; Li, S.; Milunic, D.; Bourdelle, P.; Vallejo, R. *Anal. Biochem.* **2001**, *293*, 22−30.
(18) Li, J. J.; Ouellette, A. L.; Giovangrandi, L.; Cooper, D. E.; Ricco, A. J.; Kovacs, G. T. A. *IEEE Trans. Biomed. Eng.* **2008**, *55*, 1560−1571.
(19) Huang, L.; Zhou, L.; Zhang, Y.; Xie, C.; Qu, J.; Zeng, A.; Huang, H.; Yang, R.; Wang, X. *IEEE Sens. J.* **2009**, *9*, 1185−1191.
(20) Ouellette, A. L.; Li, J. J.; Cooper, D. E.; Ricco, A. J.; Kovacs, G. T. A. *Anal. Chem.* **2009**, *81*, 3216−3221.
(21) Lakowicz, J. R. *Principles of Fluorescence Spectroscopy*, 2nd ed.; Kluwer Academic/Plenum Publishers: New York, 1999.
(22) Diamandis, E. P.; Christopoulos, T. K. *Anal. Chem.* **1990**, *62*, 1149A−1157A.
(23) Rundström, G.; Jonsson, A.; Mårtensson, O.; Mendel-Hartvig, I.; Venge, P. *Clin. Chem.* **2007**, *53*, 342−348.
(24) Ye, Z.; Tan, M.; Wang, G.; Yuan, J. *J. Mater. Chem.* **2004**, *14*, 851−856.
(25) Dekker, A. J. *Solid State Physics*; Macmillan & Co. Ltd.: London, 1962.
(26) Van den Eeckhout, K.; Smet, P. F.; Poelman, D. *Materials* **2010**, *3*, 2536−2566.
(27) Hölsä, J.; Laamanen, T.; Lastusaari, M.; Niittykoski, J.; Novák, P. *J. Rare Earths* **2009**, *27*, 550−554.
(28) Hölsa, J.; Jungner, H.; Lastusaari, M.; Niittykoski, J. *J. Alloys Compd.* **2001**, *323*−*324*, 326−330.
(29) Jia, W.; Yuan, H.; Lu, L.; Liu, H.; Yen, W. M. *J. Lumin.* **1998**, *76&77*, 424−428.
(30) Clabau, F.; Rocquefelte, X.; Jobic, S.; Deniard, P.; Whangbo, M.-H.; Garcia, A.; Mercier, T. L. *Chem. Mater.* **2005**, *17*, 3904−3912.
(31) Matsuzawa, T.; Aoki, Y.; Takeuchi, N.; Murayama, Y. *J. Electrochem. Soc.* **1996**, *143*, 2670−2673.
(32) Swart, H. C.; Terblans, J. J.; Ntwaeaborwa, O. M.; Kroon, R. E.; Mothudi, B. M. *Phys. B* **2012**, *407*, 1664−1667.
(33) Yamamoto, H.; Matsuzawa, T. *J. Lumin.* **1997**, *72*−*74*, 287−289.
(34) Zhou, L.; Jiao, H.; He, D. *Mater. Chem. Phys.* **2011**, *127*, 227−231.
(35) Si, D.; Geng, B.; Wang, S. *CrystEngComm* **2010**, *12*, 2722−2727.

(36) Zhang, R.; Han, G.; Zhang, L.; Yang, B. *Mater. Chem. Phys.* **2009**, *113*, 255−259.
(37) Chang, C.; Yuan, Z.; Mao, D. *J. Alloys Compd.* **2006**, *415*, 220−224.
(38) Maldiney, T.; Kaikkonen, M. U.; Seguin, J.; le Masne de Chermont, Q.; Bessodes, M.; Airenne, K. J.; Ylä-Herttuala, S.; Scherman, D.; Richard, C. *Bioconjugate Chem.* **2012**, *23*, 472−478.
(39) Maldiney, T.; Lecointre, A.; Viana, B.; Bessière, A.; Bessodes, M.; Gourier, D.; Richard, C.; Scherman, D. *J. Am. Chem. Soc.* **2011**, *133*, 11810−11815.
(40) Maldiney, T.; Richard, C.; Seguin, J.; Wattier, N.; Bessodes, M.; Scherman, D. *ACS Nano* **2011**, *5*, 854−862.
(41) Zhan-Jun, L.; Hong-Wu, Z.; Meng, S.; Jiang-Shan, S.; Hai-Xia, F. *J. Mater. Chem.* **2012**, *22*, 24713−24720.
(42) Godin, M.; Bryan, A. K.; Burg, T. P.; Babcock, K.; Manalis, S. R. *Appl. Phys. Lett.* **2007**, *91*, 123121.
(43) Burg, T. P.; Godin, M.; Knudsen, S. M.; Shen, W.; Carlson, G.; Foster, J. S.; Babcock, K.; Manalis, S. R. *Nature* **2007**, *446*, 1066−1069.
(44) Abrams, B. L.; Holloway, P. H. *Chem. Rev.* **2004**, *104*, 5783−5801.
(45) Aitasalo, T.; Dereń, P.; Hölsä, J.; Jungner, H.; Krupa, J.-C.; Lastusaari, M.; Legendziewicz, J.; Niittykoski, J.; Stręk, W. *J. Solid State Chem.* **2003**, *171*, 114−122.
(46) Lü, X. *Mater. Chem. Phys.* **2005**, *93*, 526−530.
(47) Zhu, Y.; Zeng, J.; Li, W.; Xu, L.; Guan, Q.; Liu, Y. *Appl. Surf. Sci.* **2009**, *255*, 7580−7585.
(48) Ji, P. T.; Chen, X. Y.; Wu, Y. Q. *Appl. Surf. Sci.* **2011**, *258*, 1888−1893.
(49) Mine, E.; Yamada, A.; Kobayashi, Y.; Konno, M.; Liz-Marzán, L. M. *J. Colloid Interface Sci.* **2003**, *264*, 385−390.
(50) Prabakar, S.; Assink, R. A. *J. Non-Cryst. Solids* **1997**, *211*, 39−48.
(51) Sanchez, J.; McCormick, A. *J. Phys. Chem.* **1992**, *96*, 8973−8979.
(52) Schmidt, H.; Scholze, H.; Kaiser, A. *J. Non-Cryst. Solids* **1984**, *63*, 1−11.
(53) Fyfe, C. A.; Aroca, P. P. *Chem. Mater.* **1995**, *7*, 1800−1806.
(54) Hermanson, G. T. *Bioconjugate Techniques*, 2nd ed.; Academic Press: London, 2008.
(55) Zhang, Z.; Berns, A. E.; Willbold, S.; Buitenhuis, J. *J. Colloid Interface Sci.* **2007**, *310*, 446−455.
(56) Atuchin, V. V.; Kesler, V. G.; Zaitsev, A. I.; Molokeev, M. S.; Aleksandrovsky, A. S.; Kuzubov, A. A.; Ignatova, N. Y. *J. Phys.: Condens. Matter* **2013**, *25*, 1−6.
(57) Rezania, A.; Johnson, R.; Lefkow, A. R.; Healy, K. E. *Langmuir* **1999**, *15*, 6931−6939.
(58) Bohn, P. W. In *Biomolecular Films. Design, Function, and Applications*; Rusling, J. F., Ed.; Marcel Dekker, Inc.: New York, 2003; pp 163−212.
(59) Xavier, K. A.; Willson, R. C. *Biophys. J.* **1998**, *74*, 2036−2045.
(60) Montgomery, D. C.; Runger, G. C. *Applied Statistics and Probability for Engineers*, 5th ed.; John Wiley & Sons, Inc.: Hoboken, 2011.
(61) Bagwe, R. P.; Hilliard, L. R.; Tan, W. *Langmuir* **2006**, *22*, 4357−4362.
(62) Malmsten, M.; Emoto, K.; van Alstine, J. M. *J. Colloid Interface Sci.* **1998**, *202*, 507−517.